

## Ultimate photovoltage in perovskite oxide heterostructures with critical film thickness

Cong Wang, Kui-juan Jin,<sup>a)</sup> Rui-qiang Zhao, Hui-bin Lu, Hai-zhong Guo, Chen Ge, Meng He, Can Wang, and Guo-zhen Yang

Beijing National Laboratory for Condensed Matter Physics, Institute of Physics, Chinese Academy of Sciences, Beijing 100190, People's Republic of China

(Received 25 March 2011; accepted 13 April 2011; published online 2 May 2011)

One order larger photovoltage is obtained with critical thicknesses of  $\text{La}_{0.9}\text{Sr}_{0.1}\text{MnO}_3$  films in both kinds of heterostructures of  $\text{La}_{0.9}\text{Sr}_{0.1}\text{MnO}_3/\text{SrTiO}_3$  (0.8 wt % Nb-doped) and  $\text{La}_{0.9}\text{Sr}_{0.1}\text{MnO}_3/\text{Si}$  fabricated at various oxygen pressures. Our self-consistent calculation reveals that the critical thickness of the  $\text{La}_{0.9}\text{Sr}_{0.1}\text{MnO}_3$  film with the ultimate value of photovoltage is just the thickness of the depletion layer of  $\text{La}_{0.9}\text{Sr}_{0.1}\text{MnO}_3$  in both heterojunctions, respectively. © 2011 American Institute of Physics. [doi:10.1063/1.3586250]

Interface region plays a crucial role in many novel physical properties of perovskite heterostructures, such as the occurring of the superconductivity at the interface layer between two insulating oxides  $\text{LaAlO}_3$  and  $\text{SrTiO}_3$ ,<sup>1,2</sup> polarization enhancement in oxide superlattices  $\text{CaTiO}_3/\text{SrTiO}_3/\text{BaTiO}_3$ ,<sup>3</sup> positive magnetoresistance<sup>4</sup> and novel photoelectric characteristics<sup>5,6</sup> in oxide heterostructures of  $\text{La}_{0.9}\text{Sr}_{0.1}\text{MnO}_3/\text{SrNb}_{0.01}\text{Ti}_{0.99}\text{O}_3$  (LSMO/SNTO) and  $\text{La}_{0.7}\text{Sr}_{0.3}\text{MnO}_3/\text{Si}$ . In this letter, we present another important role the interface region played on photoelectric effect in the heterostructures of *p*-type LSMO on the substrates of *n*-type  $\text{SrTiO}_3$  (0.8 wt % Nb-doped) (SNTO) and *n*-type Si, respectively. An ultimate value of photovoltage can be obtained in both kinds of the heterostructures with critical thicknesses of LSMO films. Our self-consistent calculation reveals that the critical thickness of the LSMO film with the ultimate value of photovoltage is just the thickness of the depletion layer of LSMO in LSMO/SNTO and LSMO/Si *p-n* heterojunctions, respectively. This conclusion is also supported by the photovoltage measurement on LSMO/Si heterostructures fabricated at two different oxygen pressures, which have different thickness of depletion layer due to the variation in oxygen vacancies and carrier concentrations in LSMO films.

LSMO films with various thicknesses were deposited on the substrates of  $\text{SrTiO}_3$  (001) (0.8 wt % Nb-doped), and *n*-type Si (001), respectively. The films were grown at 650 °C and an oxygen pressure of  $5 \times 10^{-2}$  Pa by a laser molecular beam epitaxy system using a XeCl excimer laser (wavelength of 308 nm, pulse width of 20 ns, energy density of  $2 \text{ J cm}^{-2}$ , 2 Hz). The thicknesses of LSMO thin films in all kinds of heterostructures were monitored by the *in situ* reflective high-energy electron diffraction. To gain insight into the oxygen vacancy effect, another series of LSMO/Si heterostructures were also fabricated at an oxygen pressure of  $1 \times 10^{-2}$  Pa in the same way. Figure 1 shows the x-ray diffraction pattern and high-resolution transmission electron microscopy (TEM) image of LSMO film with a thickness of 258 unit cells (u. c.) grown on SNTO substrate, from which the *c*-axis oriented epitaxial growth and sharp interface can

be seen. For photoelectrical measurements, Ohmic contacts to *p*-type semiconducting LSMO films and *n*-type semiconducting SNTO (Si) substrates were formed by using platinum electrodes on LSMO and indium electrodes on the substrates with an area of  $\sim 0.5 \text{ mm}^2$ , respectively. The photovoltaic signals were measured by a 350 MHz sampling oscilloscope with an input impedance of 1 M $\Omega$ . All the measurements were carried out at room temperature.

Figure 2(a) shows the photovoltages of *p-n* heterojunctions of LSMO/SNTO fabricated at an oxygen pressure of  $5 \times 10^{-2}$  Pa (a1), and LSMO/Si heterojunctions fabricated at oxygen pressures of  $5 \times 10^{-2}$  Pa (a2) and  $1 \times 10^{-2}$  Pa (a3).

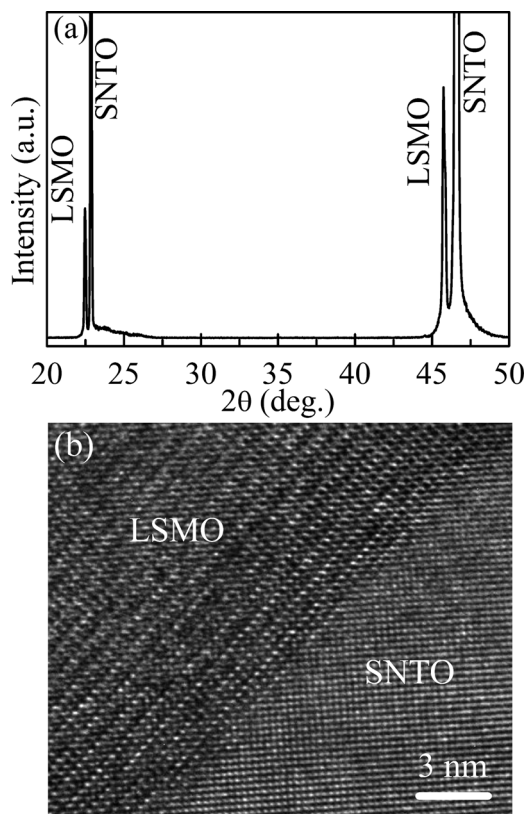


FIG. 1. (a) X-ray diffraction pattern and (b) high-resolution cross-sectional TEM image of LSMO/SNTO heterostructures with a film thickness of 258 u. c.

<sup>a)</sup> Author to whom correspondence should be addressed. Electronic mail: kjjin@aphy.iphy.ac.cn.

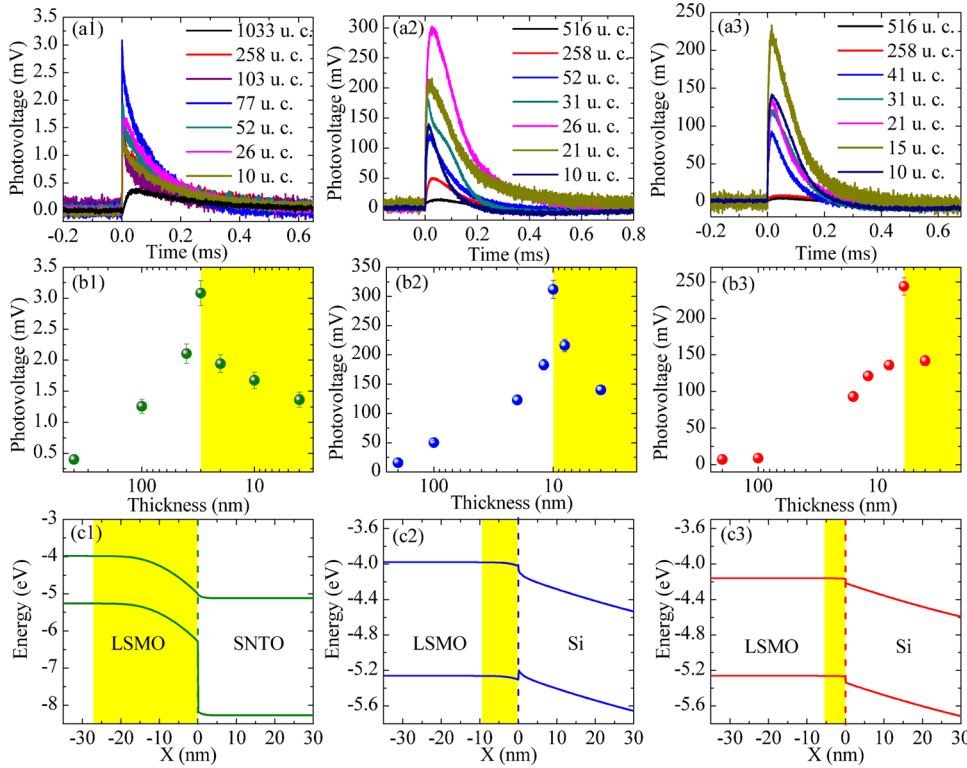


FIG. 2. (Color online) (a) Photovoltage of LSMO/SNTO heterojunctions fabricated at an oxygen pressure of  $5 \times 10^{-2}$  Pa (a1), and LSMO/Si heterojunctions fabricated at oxygen pressures of  $5 \times 10^{-2}$  Pa (a2) and  $1 \times 10^{-2}$  Pa (a3). (b) Thickness dependence of peak values of photovoltages of LSMO/SNTO heterojunctions fabricated at an oxygen pressure of  $5 \times 10^{-2}$  Pa (b1), and LSMO/Si heterojunctions fabricated at oxygen pressures of  $5 \times 10^{-2}$  Pa (b2) and  $1 \times 10^{-2}$  Pa (b3). (c) Band diagrams of LSMO/SNTO heterojunctions fabricated at an oxygen pressure of  $5 \times 10^{-2}$  Pa (c1), and LSMO/Si heterojunctions fabricated at oxygen pressures of  $5 \times 10^{-2}$  Pa (c2) and  $1 \times 10^{-2}$  Pa (c3). The yellow shadow and vertical dash line denotes the calculated depletion layer in LSMO films and the interface of these heterojunctions, respectively.

A 308 nm XeCl excimer laser (pulse width of 20 ns, energy density of  $0.02 \text{ J cm}^{-2}$ ) was used as the light source, and the electrodes were always kept in dark during the experiments to avoid possible effects. From Fig. 2(a), it can be seen that the amplitude of the photovoltage changes dramatically with the LSMO thickness for both kinds of heterostructures of LSMO/SNTO and LSMO/Si. To obtain further insight into the relation of these photovoltaic effects and the film thickness of LSMO in the heterostructures, the thickness dependences of the peak values of photovoltages of LSMO/SNTO and LSMO/Si heterojunctions are plotted in Fig. 2(b). Ultimate values of photovoltages (one order of magnitude larger than that in the heterostructures with the thickest LSMO film) are obtained in the heterostructures with critical thicknesses of LSMO thin films. These critical thicknesses of LSMO are roughly 30 nm in LSMO/SNTO, and 10 nm and 6 nm in LSMO/Si fabricated at  $5 \times 10^{-2}$  Pa and  $1 \times 10^{-2}$  Pa, respectively, as shown in Fig. 2(b).

With the decrease in the LSMO thickness from 400 nm for LSMO/SNTO (200 nm for LSMO/Si) to a few nanometers, an enhancement of one order of magnitude of the photovoltage was observed. This phenomenon can be understood in the following way. The photovoltaic effect in  $p$ - $n$  junctions is induced by the separation of photon-generated electron-hole pairs through the built-in electric field around the interfaces.<sup>7</sup> The shortening of the diffusion distance of photon-generated holes from the depletion layer to the electrode in a thinner LSMO film can greatly reduce the recombination of photon-generated holes before they are collected by the electrodes at the surface of LSMO films in the heterostructures, therefore the photovoltage increases with the decrease in LSMO thickness in the heterostructures.

From Fig. 2(b), we can also see that the photovoltage decreases with the further decrease in the thickness of LSMO for the thickness being smaller than the critical value mentioned above. In order to understand the relation of peak

photovoltage and the critical thickness of LSMO films in the heterostructures, self-consistent calculations were carried out theoretically based on the drift-diffusion model introduced in our previous works,<sup>8-10</sup> and the calculated energy-band diagrams near the interface of LSMO/SNTO and LSMO/Si heterostructures are plotted in Fig. 2(c).

In the drift-diffusion model, for a one-dimensional analysis, there are three main equations: the Poisson equation

$$\frac{d^2\psi(x)}{dx^2} = -(q/\epsilon)[p(x) - n(x) + N], \quad (1)$$

and the continuity equations

$$q[G_n(x) - U_n(x)] + \frac{dJ_n}{dx} = 0, \quad (2)$$

$$q[G_p(x) - U_p(x)] - \frac{dJ_p}{dx} = 0. \quad (3)$$

In the above equations,

$$J_n = -q \left[ \mu_n n(x) \frac{d\psi(x)}{dx} - \frac{kT}{q} \frac{dn(x)}{dx} \right], \quad (4)$$

$$J_p = -q \left[ \mu_p p(x) \frac{d\psi(x)}{dx} + \frac{kT}{q} \frac{dp(x)}{dx} \right], \quad (5)$$

$\Psi(x)$  is the electric potential,  $q$  is the elementary charge,  $\epsilon$  is the permittivity,  $N$  is the net impurity concentration,  $n(x)$  and  $p(x)$  are the electron and hole concentrations, respectively;  $G(x)$  and  $U(x)$  are the generation and recombination rates, respectively;  $J_n$  and  $J_p$  are the electron and hole current densities, respectively;  $\mu_n$  and  $\mu_p$  are the electron and hole mobilities, respectively;  $k$  and  $T$  are the Boltzmann constant and the absolute temperature, respectively.

TABLE I. The parameters used in our calculation (Refs. 9 and 11–13).

	La <sub>0.9</sub> Sr <sub>0.1</sub> MnO <sub>3</sub> (5 × 10 <sup>-2</sup> Pa)	La <sub>0.9</sub> Sr <sub>0.1</sub> MnO <sub>3</sub> (1 × 10 <sup>-2</sup> Pa)	Nb:SrTiO <sub>3</sub>	Si
Relative permittivity ( $\epsilon_0$ )	65	65	100	11.9
Affinity energy (eV)	3.98	4.16	4.00	4.05
Intrinsic carrier density (cm <sup>-3</sup> )	4.82 × 10 <sup>9</sup>	1.57 × 10 <sup>11</sup>	1.04 × 10 <sup>-4</sup>	1.5 × 10 <sup>10</sup>
Doping concentration (cm <sup>-3</sup> )	2.25 × 10 <sup>19</sup>	2.25 × 10 <sup>19</sup>	2.12 × 10 <sup>20</sup>	9.00 × 10 <sup>16</sup>
Electron mobility (cm <sup>2</sup> V <sup>-1</sup> s <sup>-1</sup> )	10	10	8	1350
Hole mobility (cm <sup>2</sup> V <sup>-1</sup> s <sup>-1</sup> )	1.8	1.8	0.1	500

The parameters we used were listed in Table I. Some of those parameters, such as doping concentrations, were obtained from our Hall measurements and others from some reference papers.<sup>9,11–13</sup> To clearly show the relation of the ultimate photovoltages and the thickness of the depletion layer, the calculated depletion layers were denoted by yellow shadow in Figs. 2(b) and 2(c). The reason that we take a larger intrinsic carrier concentration for LSMO samples fabricated at the lower oxygen pressure (1 × 10<sup>-2</sup> Pa) is that more oxygen vacancies in LSMO films fabricated at the lower oxygen pressure can be taken as higher electron doping in a hole doping semiconducting LSMO system, which can be equivalently taken as a larger intrinsic carrier concentration in this *p*-type semiconductor films. From Figs. 2(b) and 2(c), we can find out that the ultimate value of the photovoltage is just obtained in the heterostructures with LSMO thickness around the thickness of the depletion layer of LSMO. From the fact of the coincidence of the thicknesses, we can understand the phenomenon of the decrease in photovoltage with the further decreasing thickness of LSMO in the heterostructures in the following way. For LSMO films with the thickness smaller than that of the depletion layer at the interface, photovoltage decreases with the decreasing of the thickness due to the narrowing of the depletion region and the weakening of the built-in field, which was consistent with the similar phenomenon we found in LSMO/SNTO heterostructure.<sup>14</sup>

To make sure that the results are reliable, several groups of heterostructures were fabricated in the condition mentioned above and measured in the same way, which convinced that the phenomenon presented in this letter was repeatable.

In conclusion, by systematic investigation on photovoltaic effects in the heterostructures of LSMO/SNTO and LSMO/Si through varying film thicknesses and oxygen pressures, an enhancement of one order of magnitude of photovoltages in these heterojunctions was observed with decreasing the LSMO film thickness from 400 nm for LSMO/SNTO (200 nm for LSMO/Si) to a few nanometers. An ultimate value of photovoltage was found in the heterostructures with the film thickness consistent with the calculated thickness of the depletion layer in LSMO films for heterostructures of LSMO/SNTO and LSMO/Si fabricated under different oxygen pressures. We believe that the increase in the photovoltage with the decrease in the thickness of LSMO films is due to the greatly reduction in the recombination of photon-generated electrons and holes in LSMO films in the heterostructures. And the decrease in the photovoltage with the further decreasing thickness of LSMO films thinner than a critical value, the thickness of the depletion layer on the

LSMO side of the heterostructures, is resulting from the weakening of the built-in electric field and the narrowing of the depletion region around the interfaces. From this work, it can be predicted that the maximum photovoltage can be obtained in the artificially designed heterostructure with the thickness of the substrate coinciding with the depletion layer. So an artificially structure designing of the system with the thicknesses of both thin film and substrate coinciding with the thicknesses for their depletion layer, respectively, should be highly expected for the photovoltaic device.

We acknowledge the financial support of the National Natural Science Foundation of China and the National Basic Research Program of China.

<sup>1</sup>N. Reyren, S. Thiel, A. D. Caviglia, L. Fitting Kourkoutis, G. Hammerl, C. Richter, C. W. Schneider, T. Kopp, A. S. Rüetschi, D. Jaccard, M. Gabay, D. A. Muller, J. M. Triscone, and J. Mannhart, *Science* **317**, 1196 (2007).

<sup>2</sup>G. Herranz, M. Basletic, M. Bibes, C. Carretero, E. Tafra, E. Jacquet, K. Bouzehouane, C. Deranlot, A. Hamzic, J. M. Broto, A. Barthelémy, and A. Fert, *Phys. Rev. Lett.* **98**, 216803 (2007).

<sup>3</sup>H. N. Lee, H. M. Christen, M. F. Chisholm, C. M. Rouleau, and D. H. Lowndes, *Nature (London)* **433**, 395 (2005).

<sup>4</sup>H. B. Lu, S. Y. Dai, Z. H. Chen, G. Z. Yang, Y. L. Zhou, M. He, L. F. Liu, H. Z. Guo, Y. Y. Fei, and W. F. Xiang, *Appl. Phys. Lett.* **86**, 032502 (2005); K. J. Jin, H. B. Lu, Q. L. Zhou, K. Zhao, B. L. Cheng, Z. H. Chen, Y. L. Zhou, and G. Z. Yang, *Phys. Rev. B* **71**, 184428 (2005); K. J. Jin, H. B. Lu, K. Zhao, C. Ge, M. He, and G. Z. Yang, *Adv. Mater. (Weinheim, Ger.)* **21**, 4636 (2009).

<sup>5</sup>T. Muramatsu, Y. Muraoka, and Z. Hiroi, *Solid State Commun.* **132**, 351 (2004); J. R. Sun, C. H. Lai, and H. K. Wong, *Appl. Phys. Lett.* **85**, 37 (2004); J. R. Sun, B. G. Shen, Z. G. Sheng, and Y. P. Sun, *ibid.* **85**, 3375 (2004).

<sup>6</sup>H. B. Lu, K. J. Jin, Y. H. Huang, M. He, K. Zhao, B. L. Cheng, Z. H. Chen, Y. L. Zhou, S. Y. Dai, and G. Z. Yang, *Appl. Phys. Lett.* **86**, 241915 (2005); L. Liao, K. J. Jin, H. B. Lu, P. Han, M. He, and G. Z. Yang, *Solid State Commun.* **149**, 915 (2009); L. Liao, K. J. Jin, C. Ge, C. L. Hu, H. B. Lu, and G. Z. Yang, *Appl. Phys. Lett.* **96**, 062116 (2010); C. Ge, K. J. Jin, H. B. Lu, C. Wang, G. M. Zhao, L. L. Zhang, and G. Z. Yang, *Solid State Commun.* **150**, 2114 (2010).

<sup>7</sup>K. J. Jin, K. Zhao, H. B. Lu, L. Liao, and G. Z. Yang, *Appl. Phys. Lett.* **91**, 081906 (2007).

<sup>8</sup>J. Qiu, K. J. Jin, P. Han, H. B. Lu, C. L. Hu, B. P. Wang, and G. Z. Yang, *Europhys. Lett.* **79**, 57004 (2007).

<sup>9</sup>P. Han, K. J. Jin, H. B. Lu, Q. L. Zhou, Y. L. Zhou, and G. Z. Yang, *Appl. Phys. Lett.* **91**, 182102 (2007).

<sup>10</sup>C. L. Hu, P. Han, K. J. Jin, H. B. Lu, and G. Z. Yang, *J. Appl. Phys.* **103**, 053701 (2008).

<sup>11</sup>T. Fujii, M. Kawasaki, A. Sawa, Y. Kawazoe, H. Akoh, and Y. Tokura, *Phys. Rev. B* **75**, 165101 (2007).

<sup>12</sup>S. Myhajlenko, A. Bell, F. Ponce, J. L. Edward, Y. Wei, B. Craigo, D. Convey, H. Li, R. Liu, and J. Kulik, *J. Appl. Phys.* **97**, 014101 (2005).

<sup>13</sup>K. W. Böer, *Survey of Semiconductor Physics* (Van Nostrand Reinhold, New York, 1990), Vol. II.

<sup>14</sup>J. Qiu, H. B. Lu, K. J. Jin, M. He, and J. Xing, *Physica B* **400**, 66 (2007).